Published OnlineFirst February 2, 2016; DOI: 10.1158/0008-5472.CAN-15-1793

Microenvironment and Immunology

Cancer Research

Galectin-3 Cleavage Alters Bone Remodeling: Different Outcomes in Breast and Prostate Cancer Skeletal Metastasis

Kosei Nakajima[1], Dhong Hyo Kho[1], Takashi Yanagawa[2], Yosuke Harazono[3], Victor Hogan[1], Wei Chen[4], Rouba Ali-Fehmi[5], Rohit Mehra[6], and Avraham Raz[1,5]

Abstract

Management of bone metastasis remains clinically challenging and requires the identification of new molecular target(s) that can be therapeutically exploited to improve patient outcome. Galectin-3 (Gal-3) has been implicated as a secreted factor that alters the bone microenvironment. Proteolytic cleavage of Gal-3 may also contribute to malignant cellular behaviors, but has not been addressed in cancer metastasis. Here, we report that Gal-3 modulates the osteolytic bone tumor microenvironment in the presence of RANKL. Gal-3 was localized on the osteoclast cell surface, and its suppression by RNAi or a specific antagonist markedly inhibited osteoclast differentiation markers, including tartrate-resistant acid phosphatase, and reduced the number of mature osteoclasts. Structurally, the 158–175 amino acid sequence in the carbohydrate recognition domain (CRD) of Gal-3 was responsible for augmented osteoclastogenesis. During osteoclast maturation, Gal-3 interacted and colocalized with myosin-2A along the surface of cell–cell fusion. Pathologically, bone metastatic cancers expressed and released an intact form of Gal-3, mainly detected in breast cancer bone metastases, as well as a cleaved form, more abundant in prostate cancer bone metastases. Secreted intact Gal-3 interacted with myosin-2A, leading to osteoclastogenesis, whereas a shift to cleaved Gal-3 attenuated the enhancement in osteoclast differentiation. Thus, our studies demonstrate that Gal-3 shapes the bone tumor microenvironment through distinct roles contingent on its cleavage status, and highlight Gal-3 targeting through the CRD as a potential therapeutic strategy for mitigating osteolytic bone remodeling in the metastatic niche. *Cancer Res; 76(6); 1391–402. ©2016 AACR.*

Introduction

Cancer bone metastasis remains as a debilitating clinical problem in patients with prostate, breast, and other cancers that utilize either hematogenous and/or lymphatic venues. Bone colonization by disseminated cancer cells leads to communication with the host bone microenvironment. This causes bone remodeling and skeletal-related events, such as bone pain, which reduces the patient's quality of life (1, 2). Some patients with advanced metastatic lesions experience pathologic fractures or spinal cord compression. In these cases, clinical modality may include surgical intervention while considering patients' performance status and estimated prognosis (3). Radiotherapy provides an option for localized lesion and pain control. In the event of multiple cancer foci, systemic multidisciplinary treatments, including hormone therapy, chemotherapy, and bone-targeted therapy, have been utilized following bone metastasis treatment guidelines (4). Because bone metastasis is considered an incurable situation in most cases, current treatments are generally restricted to palliative management. There is an unmet need to identify treatment target(s) that orchestrate the bone tumor microenvironment (TME), and targeting such a critical molecule would be beneficial to halt and eradicate the progression of bone metastasis.

Galectin-3 (Gal-3), a lectin family protein, plays a significant role as a signaling modulator intracellularly and a potent proinflammatory protein extracellularly and is involved in cell growth, homeostasis, apoptosis, adhesion, transformation, signaling induction, angiogenesis, fibrosis, cancer progression, and metastasis (5). During the bone metastatic process, Gal-3 mediates adhesion at the interface between tumor cells and bone marrow endothelial cells (6, 7). Focusing on the bone TME, prostate and breast carcinoma secrete Gal-3, suppressing osteoblast differentiation (1), which also results in a higher serum concentration of Gal-3 in patients with breast and prostate cancer metastasis as compared with normal counterparts (8, 9). Structurally, human Gal-3 is a β-galactoside–binding protein comprising 250 amino acid residues and is a chimeric gene-product composed of three distinct structural domains: a short NH_2-terminal domain containing a phosphorylation site, a repeated collagen α-like sequence, and a

[1]Department of Oncology and Pathology, Karmanos Cancer Institute, Wayne State University, Detroit, Michigan. [2]Department of Orthopedic Surgery, Graduate School of Medicine, Gunma University, Maebashi, Gunma, Japan. [3]Maxillofacial Surgery, Department of Maxillofacial Neck Reconstruction, Graduate School of Medical and Dental Sciences, Tokyo Medical and Dental University, Bunkyo, Tokyo, Japan. [4]Biostatistics Core, Karmanos Cancer Institute, Wayne State University, Detroit, Michigan. [5]Department of Pathology, School of Medicine, Wayne State University, Detroit, Michigan. [6]Department of Pathology, University of Michigan Medical School, Ann Arbor, Michigan.

Note: Supplementary data for this article are available at Cancer Research Online (http://cancerres.aacrjournals.org/).

Corresponding Author: Avraham Raz, Wayne State University School of Medicine, Karmanos Cancer Institute, 110 E Warren Ave, Detroit, Michigan 48201. Phone: 313-578-4330; Fax: 313-831-7518; E-mail: raza@karmanos.org

doi: 10.1158/0008-5472.CAN-15-1793

Published OnlineFirst February 2, 2016; DOI: 10.1158/0008-5472.CAN-15-1793

C-terminal domain containing a single carbohydrate recognition domain (CRD) composed of 140 amino acids (10). Due to its unique molecular structure, Gal-3 was reported to be a substrate for enzymatic cleavage by matrix metalloproteinases (MMP) and prostate-specific antigen (PSA) at Gly^{32}-Ala^{33}, Ala^{62}-Tyr^{63}, and Tyr^{107}-Gly^{108} (11–13). This proteolytic modification of secretory factors is named the degradome-peptidome (14). In humans, more than 500 proteases such as MMPs and PSA and their substrates, including Gal-3, are categorized in this manner (15), any of which could significantly affect the TME. Past studies showed that the cleaved form of extracellular Gal-3 by breast and prostate carcinomas modulates angiogenesis and cell migration (12, 13) and is associated with malignancy in primary lesions (11, 16). However, the cleavage status of Gal-3 in metastatic lesions remains unclear. Therefore, we hypothesized that Gal-3 and its cleaved products could similarly affect the bone TME in breast and prostate cancer.

In the bone metastatic niche, growing cancer cells disturb the bone cellular differentiation by secretory factors affecting both osteoblasts and osteoclasts (2). Bone degradation is controlled by osteoclasts nourished in the bone TME, following which, substrates released from the bone matrix enhance cancer progression in bone, resulting in pain (2). Thus, unlike other metastatic sites, anticancer therapeutic approaches alone are not enough to treat bone metastasis and alleviate pain (17, 18). Evidence from a clinical study showed that it is significant to control not only cancer growth but also osteoclasts in metastatic bone lesions, because osteoclast targeting therapy prolonged bone metastasis–free periods (19). Importantly, the functions of osteoclasts depend on their differentiation status regulated mainly by M-CSF and RANKL (receptor activator of nuclear factor kappa-B ligand; refs. 20, 21), which induce maturation into multinucleated functional osteoclasts (osteoclastogenesis). It should be noted that M-CSF stimulation induces Gal-3 expression to be localized on plasma membranes of osteoclast precursors, suggesting a role of Gal-3 in osteoclastogenesis (22). Nevertheless, the Gal-3 function of osteoclasts in bone TME is yet to be addressed, and we hypothesized that Gal-3 may contribute to osteoclastogenesis in bone TME.

Here, we provide evidence that Gal-3 cleavage in the bone TME of breast and prostate cancers alters osteoclastogenesis, and suggest that targeting the CRD of Gal-3 may suppress bone remodeling induction by disseminated cancer cells.

Materials and Methods

Cell culture and reagents

Mouse osteoclast precursors, Raw 264.7, were purchased from the ATCC (2013), and the 2nd passage cells were used in all experiments. The cells were cultured in α-Minimum Essential Medium supplemented with 10% FBS, and the differentiation was induced by RANKL at 100 μg/mL. Human osteoclast precursors, Poietics, were purchased from Lonza (2014), and the differentiation was induced by M-CSF and RANKL following the manufacturer's protocol. The human breast cancer cell line MDA-MB-231 was a gift from Dr. Isaiah J. Fidler (University of Texas, MD Anderson Cancer Center, Houston, TX; 2005). The human breast cancer cell line T47D was a gift from Dr. Eric W. Thompson (St. Vincent's Institute of Medical Research and University of Melbourne, Melbourne, Australia; 2000). Human prostate cancer cell lines LNCaP, DU145, and PC-3 were purchased from the ATCC (2005). Customized polyclonal rabbit anti-CRD of Gal-3 antibody against amino acids 158–175 (HFNPRFNENNRR-VIVCNT) was created by Genemed Biotechnologies based on the three-dimensional (3D) structure of CRD (23) and purified by affinity chromatography using recombinant Gal-3. Monoclonal mouse anti-human RANKL-neutralizing antibody was purchased from R&D Systems. Polyclonal rabbit anti–myosin-2A antibody (MYH9, D-16) was purchased from Santa Cruz Biotechnology.

Human tissue specimens

Clinical samples were processed according to institution-approved protocols. Twenty-four biopsies of bone metastasis and 15 lesions each of other metastasis sites, including lymph node and lung originating from breast cancer primary sites plus an additional 13 biopsies of bone metastasis and 10 lesions each of other metastasis sites, including lymph node and lung originating from prostate cancer primary sites, were obtained from the Wayne State University, Department of Pathology depository. A tissue array for prostate cancer metastasis was prepared at the Department of Pathology, University of Michigan, which consists of 84 lesions from bone metastasis, including limb, spine, and rib, and 51 lesions from other metastasis sites, including lymph node, lung, liver, bladder, and other soft tissues (24). All specimens were formalin-fixed and paraffin-embedded. Due to the nature of our paired sample analysis, if only one of the two antibody measurements is available, that sample was excluded from analyses. As a result, 8 of 54 and 22 of 129 were removed for breast and prostate cancer, respectively.

Immunohistochemistry

Monoclonal rat anti-Gal-3 antibody (TIB166) against the amino terminus of Gal-3, which detects only intact Gal-3, was obtained from the ATCC. Customized polyclonal rabbit anti–Gal-3 antibody (HL31) directed against the carboxy terminus of Gal-3, which detects the cleaved Gal-3 as well as intact Gal-3, was created by Bethyl Laboratories. Immunohistochemical staining and tissue evaluation were performed as described previously (11, 16).

Transfection and plasmid constructs

si-RNA against mouse Gal-3, myosin-2A, and control si-RNA (Santa Cruz Biotechnology, shown as si-RNA No. 1 and Silencer Select; Ambion; shown as si-RNA No. 2) were transfected into each cell using Lipofectamine RNAiMax Reagent (Invitrogen). sh-RNA against Gal-3 was created using pSilencer 3.1-H1 neo expression vector (Ambion) following previous study (16). LnCaP transfectants secreting full-length (1–250 aa) and cleaved (33–250 aa, 63–250 aa) Gal-3 were generated using Lipofectamine LTX and Plus transfection reagent (Invitrogen) and p3xFLAG-MYC-CMV-25 expression vector (Sigma-Aldrich) containing a preprotrypsin leader sequence for secretion following previous study (1, 12). Recombinant Gal-3-V5 was created using the pET30as (modified pET30a) vector containing Gal-3 sequence as described (1, 13).

TRAP stain and assay

The expression and enzyme activity of TRAP, an osteoclast differentiation marker, was estimated by using a TRAP staining kit (B-Bridge International).

Published OnlineFirst February 2, 2016; DOI: 10.1158/0008-5472.CAN-15-1793

In vitro osteolysis formation assay

Human osteoclast precursors were seeded on Osteoassay surface, 96-well format (Corning) at a density of 1.0×10^4 cells in differentiation medium containing M-CSF and RANKL. After 12 hours, 500 cells of hFOB, human fetal osteoblast cells, and cancers were added. On the following day, 1 μg of each antibody was added. On sixth day, osteolytic areas were visualized by von Kossa stain and quantitated by using Image J software. For morphologic analysis, human osteoclast precursors, hFOB, and cancer cells were seeded on β-TCP (β tri-calcium phosphate) disk (3D-Biotek) in the same method as above. On sixth day, cells were fixed by 1.5% paraformaldehyde with 0.5% glutaraldehyde in 0.1 mol/L phosphate buffer for 1 hour, followed by 1% OsO_4 in 0.1 mol/L phosphate buffer for 1 hour. Then, samples were washed by 0.1 mol/L phosphate buffer and dehydrated with ethanol. After immersion in tert-butanol (2-metyl-2-propanol), samples were kept in a −20 freezer, and tert-butanol was evaporated using a vacuum evaporator. Next, ion coating was performed using gold, and then images were obtained using a Field Emission Scanning Electron Microscope, JSM-7600F (JEOL).

Statistical analysis

For a histologic evaluation of immunohistochemistry, the paired data on each patient were categorized into one of the four possible patterns, namely (0, 0), (0, 1), (1, 0), and (1, 1) for positive (1) or negative (0) as results of stain by TIB166 and HL31. Our focus is the proportion of the pattern (0, 1) named "cleaved Gal-3 pattern," and the pattern (1, 1) named "intact Gal-3 pattern" out of all possible outcomes. Summary statistics were calculated within primary cancer origin and each metastasis site. Wilson's 95% confidence intervals for the estimate of proportion were calculated. For each metastasis site, the Fisher test was performed to test the association between the origin of cancer (breast cancer and prostate cancer) and the pattern of TIB166 and HL31; odds ratios (OR) and 95% confidence intervals were calculated with conditional maximum likelihood estimation implemented in the Fisher exact test. The raw *P* values were reported, as well as the adjusted *P* values for multiple testing using false discovery rate method developed by the Benjamini and Yekutieli procedure (25). The adjusted *P* values less than 0.05 are considered statistically significant. The statistical software R 3.0 was used for immunohistochemical analyses. Other statistical analyses were performed with EZR (Saitama Medical Center, Jichi Medical University, Saitama, Japan), which is a graphical user interface for R (26). Statistical differences were determined by two sided *t*-test or one-way ANOVA with Tukey honesty significant difference (HSD) *posthoc* test.

Other methods (tissue microarray, immunofluorescence, quantitative real-time PCR, proteomics analysis, coimmunoprecipitation, coculture) were described in Supplementary Materials and Methods.

Results

Gal-3 involvement in osteoclastogenesis of bone tumor microenvironment

Initially, in order to establish the relationship of Gal-3 expression and bone metastasis, we performed immunohistochemistry with anti–Gal-3 antibody in the bone metastasis specimens obtained from prostate and breast cancer patients. Significantly, we observed the Gal-3–positive immunoreactivity in matured osteoclast lining on the bone matrix (Supplementary Fig. S1A). To find the difference of Gal-3 expression between bone metastatic lesion and primary bone tumor, we next examined Gal-3 expression in osteosarcoma, which is a major malignant tumor arising in bone, and in giant cell tumor, which is a benign osteoclast producing tumor (27). In the tissue microarray of osteosarcoma, Gal-3–positive cells appeared to congregate near the matured osteoclasts (Supplementary Fig. S1B). Similarly, in the giant cell tumor tissue array, immunoreactions with Gal-3 antibody were detected in the individual cells close to giant cells, which are excessively multinucleated osteoclast nourished by stromal cells (Supplementary Fig. S1C), and some of the Gal-3–positive cells were found to be located at the part of giant cells (Supplementary Fig. S1C'). Collectively, these findings gave evidence of Gal-3 role(s) on osteoclast differentiation in bone TME.

Gal-3 is essential for cell fusion during osteoclast differentiation

Next, we wanted to explore Gal-3 expression and its localization in osteoclast precursor cells during osteoclastogenesis. Then, we firstly examined Gal-3 expression in osteoclast precursor cells of Raw 264.7 (mouse), which also share the characteristics of monocyte/macrophage and Poietics (human), and detected in both precursors (Supplementary Fig. S2A and S2B). RANKL is a pivotal regulator controlling osteoclastogenesis in bone microenvironment and binds to the receptor, i.e., RANK on osteoclast precursors, which leads to maturation of osteoclasts (20, 21). Because osteoclast differentiation induced by RANKL is a well-established experiment *in vitro*, we employed RANKL for our culture system. Then, we investigated the endogenous Gal-3 expression and its secretion into conditioned medium during RANKL-stimulated differentiation, and found a plentiful amount of endogenous Gal-3 in both lysate and medium (Supplementary Fig. S3A). Furthermore, we examined the difference of Gal-3 localization during osteoclast differentiation, in which Raw 264.7 cells were induced by RANKL, and Poietics cells were treated with RANKL plus M-CSF. Gal-3 was mainly localized on the outer surface of osteoclasts regardless of maturation level (Fig. 1A). Next, we designed a gain of function study with recombinant Gal-3 to observe Gal-3 role in osteoclastogenesis. Since it was previously reported that the addition of recombinant Gal-3 inhibited the formation of osteoclasts (28), we firstly examined the inhibitory effect. However, we did not find the Gal-3 inhibitory effect on osteoclast differentiation in our hands. Also, recombinant Gal-3 alone was not sufficient to promote osteoclastogenesis (Supplementary Fig. S3B). Next, we addressed loss of function studies with siRNA-Gal-3 during osteoclast differentiation. Raw 264.7 cells were transiently transfected with si-Gal-3, followed by RANKL treatment, then we examined the expressional status and enzymatic activity of TRAP, a typical marker for osteoclast differentiation. The results showed that the number of TRAP-positive differentiated osteoclasts and its enzymatic activity were significantly reduced in si-Gal-3–transfected cells, indicating the contribution of Gal-3 on osteoclast differentiation (Fig. 1B and Supplementary Fig. S3C). Because the CRD of Gal-3 is responsible for multifunctionality of Gal-3 (10), we examined whether the CRD is required for the Gal-3 function on osteoclast differentiation, lactose, a CRD binding carbohydrate was added into the culture medium during osteoclast differentiation. In cells treated with lactose, the number of TRAP-positive osteoclast cells and its enzymatic activity were noticeably reduced, compared with the

Published OnlineFirst February 2, 2016; DOI: 10.1158/0008-5472.CAN-15-1793

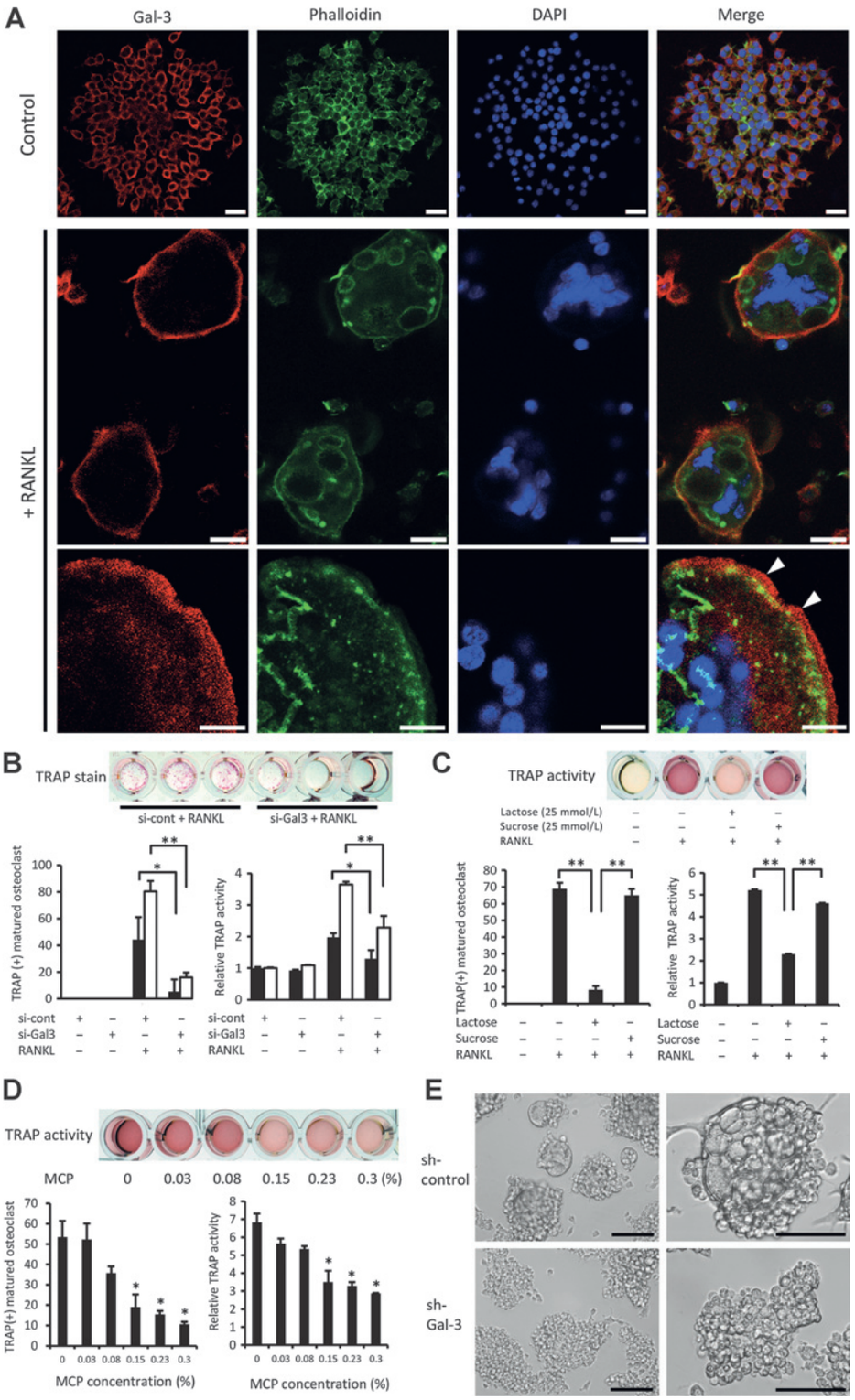

Figure 1.
Gal-3 is essential for cell fusion during osteoclast differentiation. A, Gal-3 expresses mouse osteoclast cells on the cell surface. Raw 264.7 cells were stained with or without RANKL exposure. Cells were fixed at 3 days after treatment. Images are shown Gal-3 (Alexa Fluor 680, red), phalloidin (FITC-conjugated, green), and 4′, 6-diamidino-2-phenylindole (DAPI; nuclear stain, blue). Arrowhead, expression of Gal-3 on the cell surface. White scale bar, 20 μm. B, raw 264.7 cells were cultured at 10,000 cells/well on 96-well plate and transfected with 10 nmol/L of si-Control or si-Gal-3 continuously until the following measurement. On the next day of transfection, RANKL was added. TRAP stain/assay was performed at 3 days after RANKL exposure. One-way ANOVA and Tukey HSD *posthoc* test were used for statistical analysis. Black bar, treated by si-Gal-3 (No. 1). White bar, treated by si-Gal-3 (No. 2). The inhibited protein expressions are shown in Supplementary Figure S3C. C, raw 264.7 cells were cultured at 10,000 cells/well on 96-well plate. After 8 hours, RANKL was added with lactose (25 mmol/L) or sucrose (25 mmol/L). TRAP stain and its enzymatic activity were examined at 4 days after RANKL exposure. Red color, expression of TRAP. One-way ANOVA and Tukey HSD *posthoc* test were used for statistical analysis. D, raw 264.7 cells were cultured at 10,000 cells/well on 96-well plate. After 8 hours, RANKL was added with MCP in a dose-dependent manner. TRAP stain and its enzymatic activity were examined at 4 days after RANKL exposure. Red color, expression of TRAP. Two sided t-test was used for statistical analysis compared with positive control (without MCP). E, raw 264.7 cells were transfected with sh-control vector or sh-Gal-3, and transfected clone was selected using 600 μg/mL of G418. Gal-3 knockdown was confirmed by RT-PCR and immunoblot (data not shown). After selection, RANKL was added, and then morphology of the cells was observed by inverted phase contrast microscope. Scale bar, 100 μm. Data represent mean ± SD. *, $P < 0.05$; **, $P < 0.001$.

cells treated with sucrose (control disaccharide; Fig. 1C). To validate the responsibility of Gal-3 CRD, we additionally used a Gal-3 antagonist, i.e., MCP (also known as GCS-100; refs. 29, 30). As predicted, MCP also inhibited osteoclastogenesis in a dose-dependent manner (Fig. 1D). Next, we created Gal-3 downregulated Raw 264.7 cells stably transfected with sh-Gal-3 and

Published OnlineFirst February 2, 2016; DOI: 10.1158/0008-5472.CAN-15-1793

examined how cells progress in response to RANKL. Interestingly, we observed that these established Gal-3 knockdown clones showed a deficient phenotype for cell fusion despite of RANKL stimulation (Fig. 1E). These results suggested that endogenous Gal-3 in osteoclast cells plays a crucial role during the process of cell fusion and differentiation.

CRD of extracellular Gal-3 regulates osteoclast differentiation

Because Gal-3 was intensely detectable in osteoclast culturing medium (Supplementary Fig. S3A), results of the lactose-based study (Fig. 1C) made us question whether extracellular Gal-3 participates in osteoclastogenesis. To answer this, we generated anti-CRD antibody against the 158 aa–175 aa motif harboring the CRD, and purified the antibody with antigen-based affinity chromatography and tested whether anti-CRD antibody binds to CRD (Supplementary Fig. S4). Next, we explored whether anti-CRD antibody inhibits osteoclastogenesis in comparison with anti–RANKL-neutralizing antibody, which is clinically well established for the inhibition of osteoclast differentiation. Expectedly, the results showed that anti-CRD antibody obviously reduced the number of TRAP-positive multinucleated cells and its enzymatic activity (Fig. 2A–C). Intriguingly, anti-CRD antibody reduced the number of TRAP-positive multinucleated cells and TRAP enzymatic activity relatively less than anti-RANKL antibody in our tested condition (Fig. 2A–C). Subsequently, we validated whether anti-CRD antibody also inhibits the expression of osteoclasts' differentiation makers, including the transcriptional regulators of *C-fos* and *Nfat-c1* and the executors of *Acp5*, *Ctsk*, and *Dc-stamp*

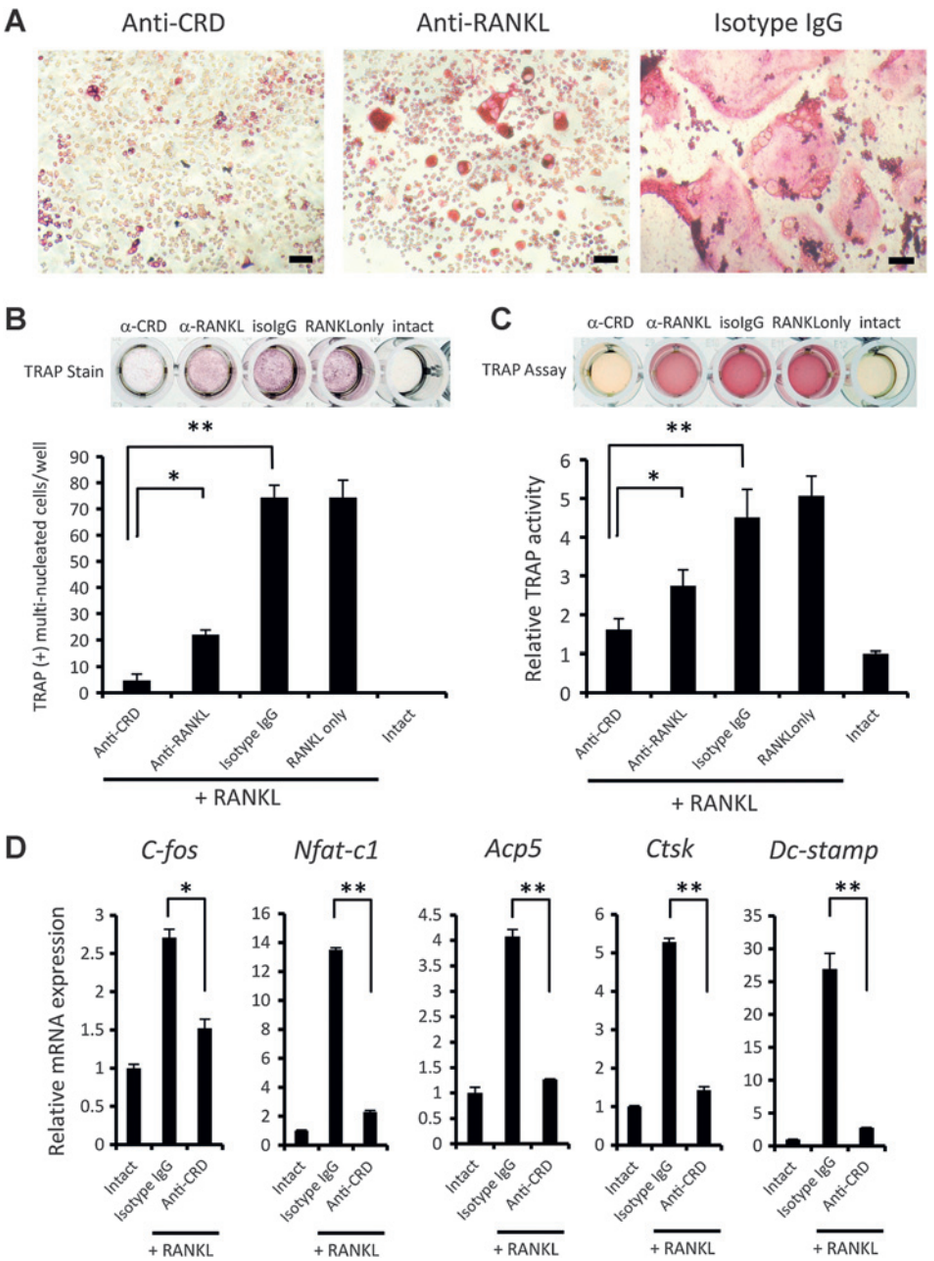

Figure 2.
CRD of extracellular Gal-3 regulates osteoclast differentiation. A–C, raw 264.7 cells were cultured at 10,000 cells/well on 96-well plate. After 8 hours, human RANKL was added with 0.5 μg of isotype IgG/anti-RANKL antibody/anti-CRD antibody. Then, TRAP stain was performed and photographed (A and B) and its enzymatic activity was examined (C) at 4 days after RANKL exposure. Red color, expression of TRAP. Scale bar, 100 μm. D, anti-CRD antibody inhibits the expression of osteoclasts' differentiation makers. RNA samples were extracted at 4 days after the addition of RANKL with isotype IgG or anti-CRD antibody. As osteoclast differentiation markers, *C-fos*, *Nfat-c1*, *Acp5*, *Ctsk*, and *Dc-stamp*, were evaluated, and mRNA levels were determined by quantitative real-time PCR. Results are presented as fold changes compared with the intact cells. One-way ANOVA and Tukey HSD *posthoc* test were used for all statistical analysis. Data represent mean ± SD. *, $P < 0.05$; **, $P < 0.001$.

Published OnlineFirst February 2, 2016; DOI: 10.1158/0008-5472.CAN-15-1793

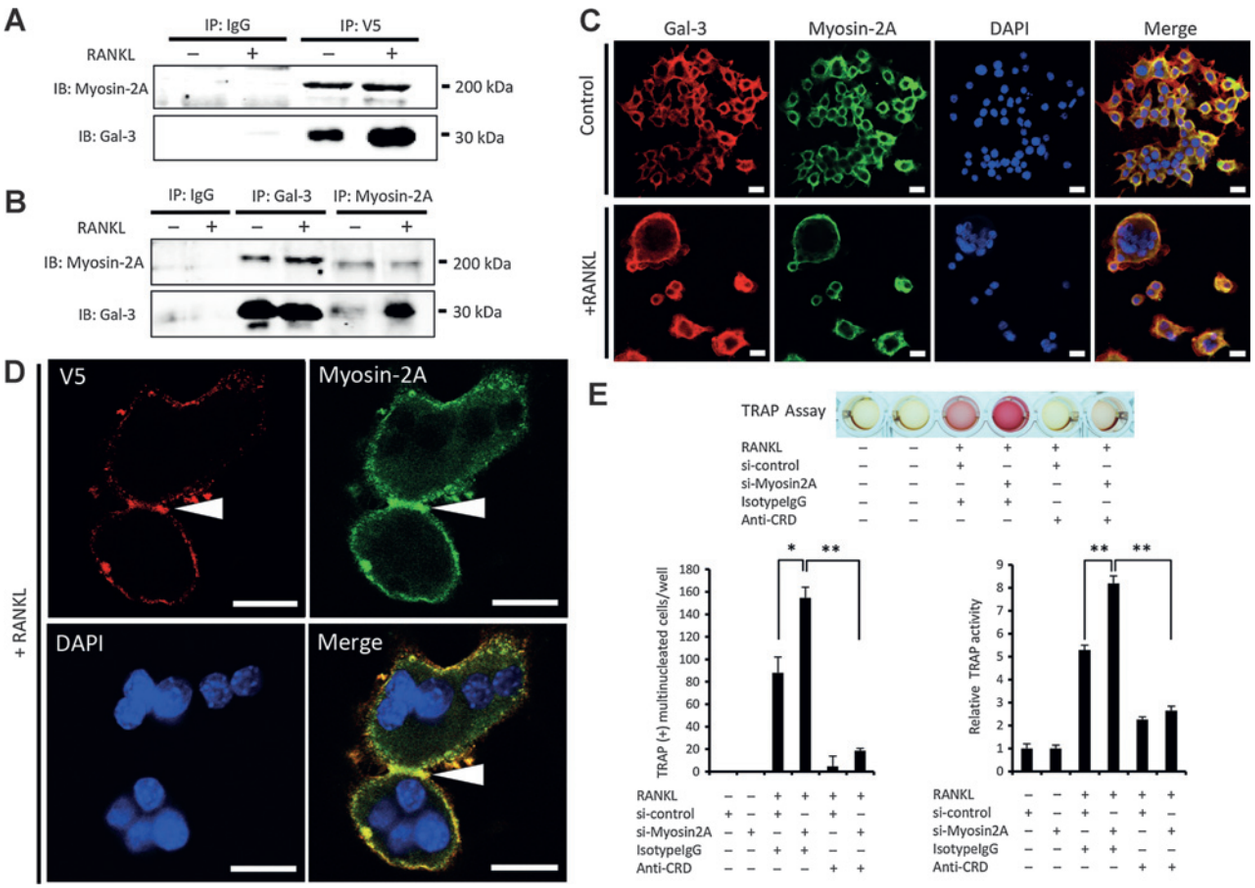

Figure 3.

Myosin-2A is a binding partner of Gal-3 for osteoclast differentiation. A, at 2 days after the addition of RANKL, purified recombinant Gal-3-V5 (1 μmol/L) was added and incubated for 1 hour, then cross-linked by 3,3′-dithiobis sulfosuccinimidyl propionate (DTSSP). Cells were lysed with Mem-PER. And then, cell lysates were immunoprecipitated with anti-V5 antibody or control IgG. Immunoprecipitates were analyzed by immunoblotting with anti–myosin-2A antibody or TIB166. B, at 2 days after the addition of RANKL, total cell lysate was extracted by 1% NP40 lysis buffer. And then, cell lysates were immunoprecipitated with TIB166, anti–Gal-3 antibody, or anti–myosin-2A antibody with control IgG. Immunoprecipitates were analyzed by immunoblotting with anti–myosin-2A antibody or TIB166. C, raw 264.7 cells were stained with or without RANKL exposure. Cells were fixed at 3 days after treatment. Images of Gal-3 (Alexa Fluor 680, red), myosin-2A (FITC, green), and 4′, 6-diamidino-2-phenylindole (DAPI; nuclear stain, blue) are shown. Scale bar, 20 μm. D, raw 264.7 cells were stained at 2 days after RANKL exposure. Cells were fixed after the incubation of recombinant Gal-3-V5 (1 μmol/L) for 1 hour. Images are shown, recombinant Gal-3-V5 (Texas-Red, red), myosin-2A (FITC, green), and 4′, 6-diamidino-2-phenylindole (DAPI; nuclear stain, blue). Scale bar, 20 μm. E, raw 264.7 cells were cultured at 10,000 cells/well on 96-well plate, then after 8 hours, transfected with 10 nmol/L of si-Control or si-myosin-2A (No. 1). On following day, RANKL was added with anti-CRD antibody or isotype IgG. TRAP (+) multinucleated cell and its enzymatic activity were examined at 3 days after RANKL exposure. Red color, expression of TRAP. The inhibited protein expressions were shown in Supplementary Fig. S5B. The results of si-myosin-2A (No. 2) are shown in Supplementary Fig. S5C. One-way ANOVA and Tukey HSD *posthoc* test were used for statistical analysis. Data represent mean ± SD. *, $P < 0.05$; **, $P < 0.001$.

(31, 32). *C-fos* was identified as a key regulator and caused a linage shift toward osteoclastogenesis in macrophage (33). *Nfat-c1* regulates a number of crucial osteoclast-specific genes, including *Acp5* and *Ctsk* (34, 35). *Acp5* encodes TRAP, which is a highly expressed enzyme in matured osteoclasts, known as a typical marker for osteoclast differentiation (36). *Ctsk* encodes cathepsin K, which is a matrix-degrading proteinase involved in bone remodeling and resorption on lacunae (37). *Dc-stamp* was identified as an essential regulator of osteoclast and macrophage cell fusion, which especially acts at later stage during fusion process (38). Quantitative real-time PCR analysis indicated that anti-CRD antibody downregulated mRNA levels of these genes (Fig. 2D), suggesting that extracellular Gal-3 affects the transcription of osteoclast differentiation markers.

Myosin-2A is a binding partner of Gal-3 for osteoclast differentiation

To understand how extracellular Gal-3 affects osteoclast differentiation, we needed to identify the extracellular Gal-3 interacting protein in osteoclast cells. Thus, we performed immunoprecipitation studies with recombinant Galectin-3-V5 (Gal-3-V5) as a bait. We found Gal-3 interacting proteins and submitted it to mass spectrometric analysis. The Gal-3 interacting protein was identified as myosin-2A ($P = 0.044$; Protein accession no. MYH9_MOUSE, Q8VDD5), which is reported to play as a modulator in osteoclast differentiation (Supplementary Fig. S5A; ref. 39). To confirm interaction of Gal-3 and myosin-2A, we treated the cells with recombinant Gal-3-V5 and carried out immunoprecipitation with anti–myosin-2A antibody, and the

Published OnlineFirst February 2, 2016; DOI: 10.1158/0008-5472.CAN-15-1793

result showed that exogenous recombinant Gal-3-V5 more intensely interacted with myosin-2A after RANKL exposure (Fig. 3A). Next, we wanted to know their endogenous interaction and performed coimmunoprecipitation using osteoclast precursor cell lysates with/without RANKL treatment. As a result, Myosin-2A was coprecipitated with Gal-3 (Fig. 3B). The reciprocal experiment showed that Gal-3 bound with myosin-2A was apparently increased in response to RANKL (Fig. 3B), indicating that Gal-3/myosin-2A interaction is enhanced during osteoclast differentiation. To visualize their interaction in cells during osteoclast differentiation, confocal immunofluorescence analysis was utilized and showed the colocalization of endogenous Gal-3 and myosin-2A on the cell surface, but no difference of colocalization pattern following RANKL stimulation and the differentiation process (Fig. 3C). Further, to distinguish between cytosolic and secreted Gal-3 in myosin-2A interaction, we used exogenous recombinant Gal-3-V5 and performed immunofluorescence analysis. Interestingly, exogenous recombinant Gal-3-V5 was also colocalized with myosin-2A at the cell surface, and both proteins strongly bound on the contact region of fused cells (Fig. 3D). The result suggested that secreted Gal-3 modulates the role of Myosin-2A in the cell fusion process during osteoclast differentiation. Indeed, myosin-2A knockdown and overexpression studies reported that myosin-2A inhibits osteoclast precursor fusion (39). Therefore, next we wanted to understand how the positive role of Gal-3 affects a negative regulator of myosin-2A during osteoclast differentiation and designed the experiment combined with si-RNA-myosin-2A and anti–Gal-3 antibody (Fig. 3E and Supplementary Fig. S5B and S5C). In accordance with a previous report of myosin-2A inhibitory effect on osteoclast differentiation (39), si-RNA-myosin-2A enhanced the number of TRAP-positive multinucleated cells and its enzymatic activity (Fig. 3E). Also, si-RNA-myosin-2A–enhancing osteoclast differentiation was suppressed by anti-CRD antibody (Fig. 3E). In other words, anti-CRD antibody inhibits osteoclast differentiation regardless of the expression level of myosin-2A. These data showed the pattern of epistasis that besides Gal-3 affects osteoclast differentiation through myosin-2A, Gal-3 is likely to play an additional role, independent of myosin-2A, ultimately resulting in the enhancement of osteoclast differentiation.

Cancer-secreted Gal-3 enhances osteoclastogenesis

Given that extracellular Gal-3 regulates osteoclast differentiation in a physiologic setting (Figs. 2 and 3), cancer-secreted Gal-3 could play a crucial role in a pathophysiologic setting, i.e., bone tumor microenvironment. First, we checked Gal-3 secretion in conditioned media cultured with metastatic breast and prostate cancer. As reported, secreted Gal-3 was detected in two forms: intact secreted Gal-3 and cleaved Gal-3 (Fig. 4A; refs. 11–13). Although Gal-3 cleavage by MMPs is suggested to be an active process during tumor progression (11, 12), no experimental evidence of cleaved Gal-3 functionality in osteoclastogenesis has been provided so far. Thus, before delineating the functional activity of cleaved Gal-3 on osteoclast differentiation, we initially examined whether cleaved Gal-3 is also able to interact with myosin-2A. Immunoprecipitation assay using conditioned media above showed that the intact form of Gal-3 binds to myosin-2A, but the cleaved form did not (Fig. 4B), implying that cleaved Gal-3 loses the ability of intact Gal-3 to bind with myosin-2A. Next, we generated the cells stably transfected with N-terminal deletion mutants (33–250 aa, 63–250 aa) mimicking cleaved Gal-3 and intact Gal-3 sequence (1–250 aa) and mimicking secretion by cancer cells (1, 12). In addition, we wanted to avoid the endogenous Gal-3 effect and employed LNCaP, a human prostate cancer

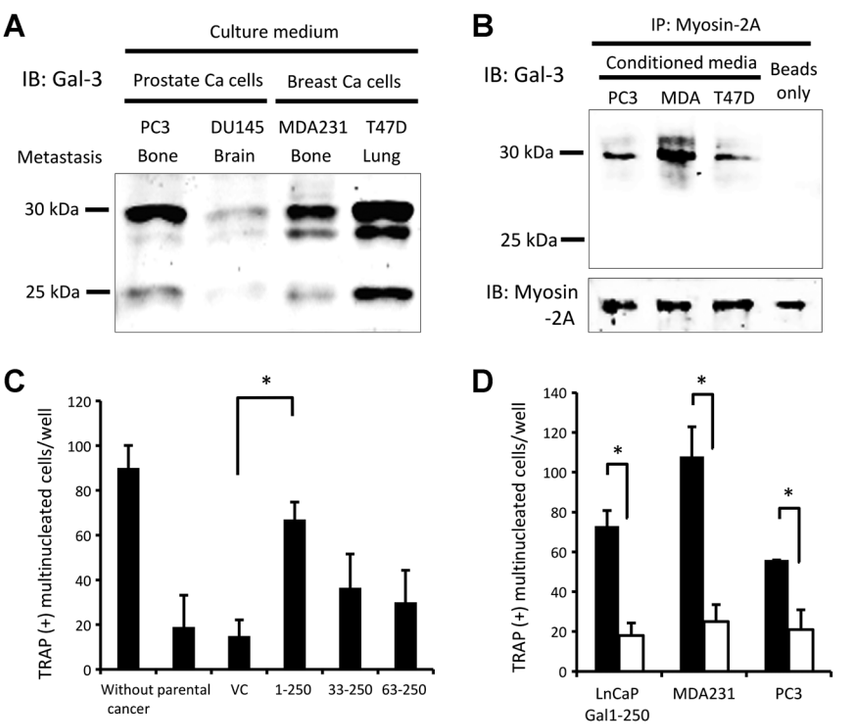

Figure 4.
Cancer-secreted Gal-3 enhances osteoclastogenesis. A, secreted/cleaved Gal-3 in human metastatic cancers. Each cancer cell was cultured with conditioned medium for 24 hours; next, the medium was concentrated to 20-fold, and then it was subjected to immunoblot. B, HeLa cell lysate (200 μg; containing myosin-2A) was incubated with 1 μg of anti–myosin-2A antibody, and then protein G Sepharose beads was added. After extensively washing the beads, it was added into 5 mL of conditioned medium, which cultured with cancer cells for 24 hours. After reaction overnight, the beads were washed and suspended in SDS sample buffer with heat. Supernatants were subjected to SDS-PAGE and immunoblot. C, raw 264.7 osteoclast precursors were cultured in the 24-well plate at 15,000 cells/well. After 8 hours, each cancer transfectant was seeded at 5,000 cells on the inserts. On following day, RANKL was added to each well. One-way ANOVA and Tukey HSD *posthoc* test were used for statistical analysis. D, raw 264.7 osteoclast precursors were cultured in the 24-well plate at 15,000 cells/well, and after 8 hours, cancer cells were seeded at 5,000 cells on the inserts. On following day, RANKL was added to each well with anti-CRD antibody or isotype IgG at 3 μg/mL. Two sided t-test was used for statistical analysis compared with isotype IgG. Black bar, treated by isotype IgG. White bar, treated by anti-CRD antibody. Data represent mean ± SD. *, $P < 0.05$.

Published OnlineFirst February 2, 2016; DOI: 10.1158/0008-5472.CAN-15-1793

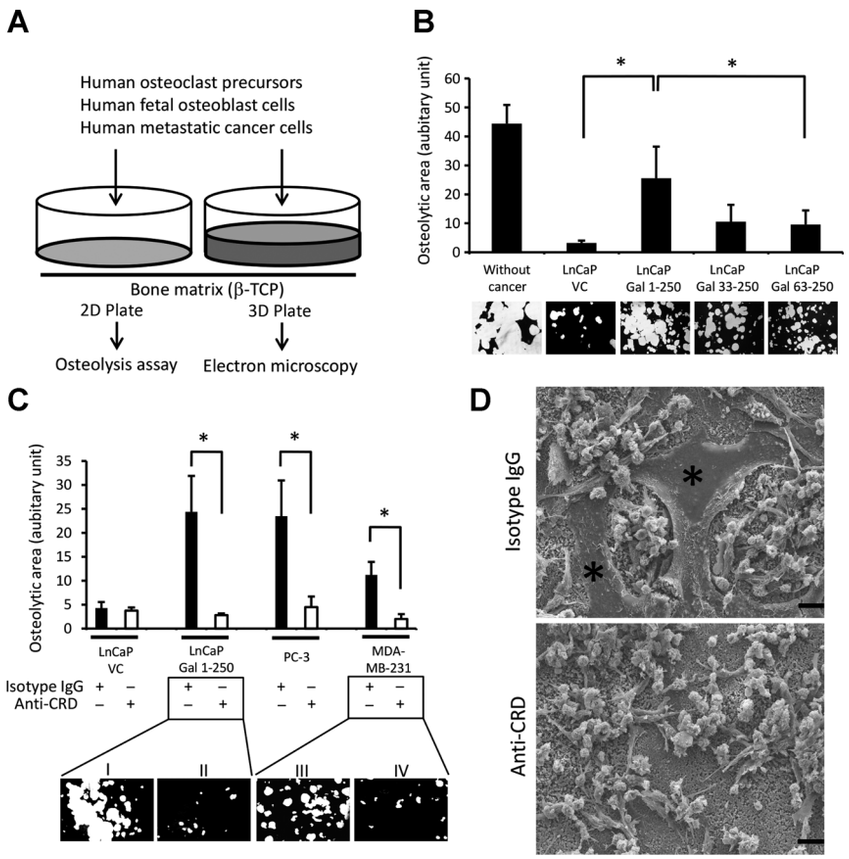

Figure 5.
Targeting CRD of Gal-3 suppresses osteolytic bone remodeling. A, schematic representation of *in vitro* osteolysis assay using β-TCP. B–C, on day 1, Poietics human osteoclast precursors were cultured in the 96-well format of β-TCP plate at 10,000 cells/well in the differentiation medium containing RANKL and M-CSF, and after 8 hours, hFOB human osteoblast cells and cancer cells were seeded at 500 cells/well. Anti-CRD antibody or isotype IgG was added to each well at 3 μg/mL on days 2 and 5. Then, von Kossa stain was performed on day 7. The visualized pit halls (white area) were photographed and measured by Image J software. One-way ANOVA and Tukey HSD *posthoc* test were used for B, whereas two sided t-test was used for C compared with isotype IgG. Data represent mean ± SD. *, $P < 0.05$. Osteolytic area was photographed and is shown below the each bar. I–II, coculture with LNCaP transfectant (Gal-3 1–250 amino acids secretable clone) treated with isotype IgG (black bar, I) or anti-CRD (white bar, II). III–IV, coculture with MDA-MB-231, which secretes/cleaves endogenous Gal-3 treated with isotype IgG (black bar, III) or anti-CRD (white bar, IV). D, on day 1, Poietics human osteoclast precursors were cultured onto the center, top surface of 3D β-TCP plate at 10,000 cells/30 μL of the differentiation medium containing RANKL and M-CSF. After 3 hours, hFOB human osteoblast cells and cancer cells were seeded at 500 cells on the plate for another 3 hours, then additionally 170 μL of differentiation medium was added (modified company's protocol). Anti-CRD antibody or isotype IgG was added to each well at 3 μg/mL on days 2 and 5. Then, cells were fixed for observation by scanning electron microscope on day 7. *, matured osteoclast.

cell line in which endogenous Gal-3 was not detected under tested conditions (1). Then, we examined how cancer-secreting truncated Gal-3 affects osteoclast differentiation in coculture system. As shown in Fig. 4C, LNCaP parental cells suppressed the formation of TRAP-positive multinucleated cells, compared with the control (no cancer cells), indicating that LNCaP cells showed the inhibitory effect on osteoclast cells as a net result of osteoclast differentiation. Interestingly, in coculturing with Gal-3 (1–250 aa)–transfected cancer cells, secreted Gal-3 overrode the LNCaP-inhibitory effect and recovered the formation of TRAP-positive multinucleated cells in osteoclast cells (Fig. 4C). This result indicated that cancer-secreting Gal-3 can regulate osteoclast differentiation, which is different from the previous observation that recombinant Gal-3 did not affect the differentiation (Supplementary Fig. S3B). We also observed that compared with intact Gal-3, N-terminal deletion mutants did not show a dominant negative effect, competing against intact Gal-3 secreted by osteoclast cells. Instead, these mutants slightly recovered TRAP positivity, indicating that truncated mutants showed, in part, the characteristics of intact Gal-3 activity (Fig. 4C). Thus, we suggest that a shift of intact Gal-3 to cleaved Gal-3 might result in a reduction of total Gal-3 activity, and the cleavage can attenuate osteoclast differentiation.

As the inducible effect of both intact and cleaved Gal-3 derived from cancer cells on osteoclast differentiation was shown, we next examined therapeutic efficiency of anti-CRD antibody on suppression of osteoclastogenesis in coculture systems mimicking the interactions of metastatic cancer cells and osteoclast cells. Expectedly, the treatment of anti-CRD antibody significantly reduced the formation of TRAP-positive multinucleated cells in coculture with Gal-3 (1–250 aa)–overexpressing LNCaP transfectant (Fig. 4D). We found similar result in bone metastatic prostate cancer PC-3 cells, and breast cancer MDA-MB-231 cells, which express endogenously both

Published OnlineFirst February 2, 2016; DOI: 10.1158/0008-5472.CAN-15-1793

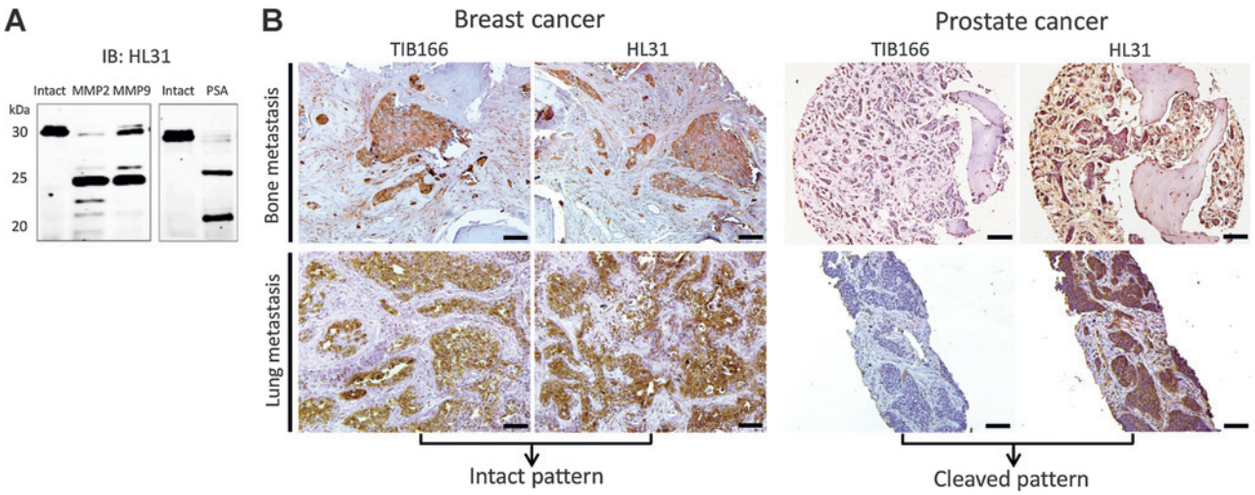

C Intact Gal-3

Metastasis	Pattern	Breast N (%)	Prostate N (%)	OR (95% CI)	*P* value	Adjusted *P* value
Bone	Intact pattern	13 **(76%)**	10 **(13%)**	0.048 (0.010,0.194)	<0.001	**<0.001**
	Others	4 (24%)	67 (87%)	Reference		
Lung	Intact pattern	7 (50%)	1 (7%)	0.085 (0.002,0.868)	0.033	0.121
	Others	7 (50%)	13 (93%)	Reference		
Lymph node	Intact pattern	10 (67%)	5 (31%)	0.239 (0.039,1.268)	0.076	0.222
	Others	5 (33%)	11 (69%)	Reference		

Cleaved Gal-3

Metastasis	Pattern	Breast N (%)	Prostate N (%)	OR (95% CI)	*P* value	Adjusted *P* value
Bone	Cleaved pattern	2 **(12%)**	57 **(74%)**	20.594 (4.234,200.793)	<0.001	**<0.001**
	Others	15 (88%)	20 (26%)	Reference		
Lung	Cleaved pattern	2 **(14%)**	10 **(71%)**	13.245 (1.787,175.937)	0.006	**0.031**
	Others	12 (86%)	4 (29%)	Reference		
Lymph node	Cleaved pattern	5 (33%)	7 (44%)	1.533 (0.290,8.641)	0.716	1
	Others	10 (67%)	9 (56%)	Reference		

Figure 6.
Breast and prostate cancer expresses intact/cleaved Gal-3 in bone metastasis. A, cleavage of Gal-3 by MMP and PSA. Recombinant Gal-3 (50 ng) was incubated for 1 hour at 37°C with proMMP-2 or proMMP-9 activated by APMA. PSA was used in EDTA (100 mmol/L)/PBS buffer, and reacted with 50 ng of recombinant Gal-3 for 6 hour at 37°C. B, distribution of intact/cleaved Gal-3 in clinical samples of patients with metastasis. Intact Gal-3 was detected by TIB166, whereas intact and cleaved Gal-3 was detected by HL31. Representative staining is shown. In breast cancer metastasis, specimens were positive by using both TIB166 and HL31, referred to as intact Gal-3 pattern, whereas in prostate cancer metastasis, specimens were negative for TIB166, but positive for HL31, referred to as cleaved Gal-3 pattern. Scale bar, 100 μm. C, statistical analysis in clinical samples of patients with metastasis. Total case numbers of each pattern (N) and percent positive of stained samples (%) are shown. Top table, association between cancer origin and pattern of paired results of TIB166 and HL31; intact Gal-3 pattern (1.1; positive TIB166 and positive HL31) vs. other pattern (including 0.0, 0.1, 1.0). Bottom table, association between cancer origin and pattern of paired results of TIB166 and HL31; cleaved Gal-3 pattern (0.1; negative TIB166 but positive HL31) vs. other pattern (including 0.0, 1.1, 1.0). In bone metastasis, the odds of prostate cancer having intact Gal-3 pattern was lower ($P < 0.001$) and the odds of cleaved Gal-3 pattern was higher than that of breast cancer ($P < 0.001$), indicating that the shift from intact to cleaved Gal-3 occurs in the prostate cancer bone metastatic niche. On the other hand, in lung and lymph node metastasis, Gal-3 cleavage shifts were not obvious.

intact and cleaved Gal-3 into culture media (Fig. 4D). It is a remarkable point that anti-CRD antibody could exert effectively suppression on osteoclast differentiation in bone TME.

Targeting CRD of Gal-3 suppresses osteolytic bone remodeling

We further investigated the effect of Gal-3 on bone destruction by osteoclasts. As shown in Fig 5A, we cocultured human osteoclast precursors, human osteoblast cells, and human cancer cells on artificial bone matrix, i.e., β-TCP, beta-tricalcium phosphate, to mimic the *in vivo* condition of bone TME. In accordance with the number of TRAP-positive multinucleated cells in Fig. 4C, LNCaP cells suppressed the osteolytic area compared to the differentiated condition without cancer cells (Fig. 5B). Consistent with Fig. 4C, Gal-3 (1–250 aa)–overexpressing LNCaP cells recovered osteolytic area, and deletion mutants (33–250 aa, 63–250 aa) expressing cancer cells slightly recovered (Fig. 5B), indicating that secreted Gal-3 enhanced osteolytic lesion, overcoming LNCaP-suppressing osteolysis. As shown in TRAP staining experiments (Fig. 4D), anti-CRD antibody markedly reduced the osteolytic area (Fig. 5C). To further detail anti-CRD antibody–mediated therapy, scanning electron microscopy allowed us to observe the 3D morphologic changes of human osteoclasts on the

Published OnlineFirst February 2, 2016; DOI: 10.1158/0008-5472.CAN-15-1793

destruction of bone matrix. We found that anti-CRD antibody maintained the osteoclast precursors in an undifferentiated state, whereas in control IgG-treated condition, osteoclast precursors typically formed an osteoclast shape (Fig. 5D). We also observed that osteoclast precursors expanded filopodia and aggregated with each other in response to RANKL stimulation, regardless of anti–Gal-3 antibody treatment (Supplementary Fig. S6). However, anti–Gal-3 CRD treatment seems to block the osteoclast cell fusion, resulting in spheroidal cell clusters instead of flattened cells by maturation (Supplementary Fig. S6). Collectively, anti–Gal-3 CRD antibody is considered as a promising therapeutic agent, suppressing metastatic cancer-induced osteolytic bone remodeling.

Gal-3 expression in bone metastasis TME

Preliminary immunohistochemistry (Supplementary Fig. S1) and *in vitro* findings of Gal-3 cleavage effect on osteoclastogenesis and its therapeutic potentiality (Fig. 4 and 5) led us to profile relative intact and/or cleaved Gal-3 in bone metastatic and other metastatic tissues. Because it has been reported that Gal-3 is cleaved by MMPs, enzymatic modulators in TME and PSA, a protease known as a tumor maker elevated in prostate cancer patient serum (11–13), we confirmed Gal-3 cleavage by these two enzymes (Fig. 6A). Previously, we demonstrated the promising detection power with two anti–Gal-3 antibodies to distinguish expression pattern between intact and cleaved Gal-3 (11, 16), i.e., we purified IgG from antiserum, in which TIB166 antibody recognized intact Gal-3 but did not bind to cleaved Gal-3, whereas HL31 antibody recognized intact as well as the cleaved form of Gal-3 (Supplementary Fig. S7A). After that, we obtained approximately 210 paraffin-embedded tissues from metastatic lesions of breast and prostate carcinomas in human patients, including lymph node, lung, and bone. We serially sectioned two slides, allowing us to stain them with each antibody. As shown in Fig. 6B and Supplementary Fig. S7B, the staining was evaluated as 0 = negative, 1 = positive. To organize the staining pattern of the two antibodies (TIB166, HL31), both TIB166 and HL31 positive refer to an intact Gal-3 pattern (1, 1); TIB166 negative and HL31 positive refer to a cleaved Gal-3 pattern (0, 1); and negative Gal-3 expression (0, 0) is both TIB166 and HL31 negative (Fig. 6B and Supplementary Fig. S7B). Then, we analyzed statistically whether the significance of Gal-3 cleavage occurs between breast and prostate cancers in each metastatic niche. In bone metastasis, the odds of prostate cancer having intact-Gal-3 pattern (1, 1) is much lower than that of breast cancer [OR, 0.048; 95% confidence interval (CI), 0.010–0.194; Fisher exact *P* value <0.001; adjusted *P* value <0.001; Fig. 6C). In contrast, the odds of prostate cancer having cleaved Gal-3 pattern (0, 1) in bone metastasis is much higher than that of breast cancer (OR, 20.594; 95% CI, 4.234–200.793; Fisher exact *P* value <0.001; adjusted *P* value < 0.001; Fig. 6C). The results indicated that the shift from intact to cleaved Gal-3 occurs in the prostate cancer bone metastatic niche more than in the breast cancer bone metastatic niche. In lung metastasis, the odds of prostate cancer having cleaved Gal-3 is much higher than the odds of breast cancer (OR, 13.245; 95% CI, 1.787–175.937; Fisher exact *P* value = 0.006; adjusted *P* value = 0.031); however, there was no significant reduction in intact Gal-3 expression (Fig. 6C), indicating that Gal-3 cleavage shift is not obvious in lung metastasis. In lymph node metastasis, no significant difference in intact and cleaved Gal-3 expression was observed (Fig. 6C). Taken together, it is likely that proteolytic shift from intact to cleaved Gal-3 is a characterized event in bone metastatic niche of prostate cancer.

Discussion

The data presented here demonstrated that cancer-secreted Gal-3 plays a crucial role in osteoclast differentiation in the presence of RANKL. RANKL is a pivotal regulator of osteoclastogenesis produced by osteoblasts, cancer cells, and activated immune cells in the bone marrow (40, 41). During osteoclast maturation, extracellular Gal-3 mediates osteoclast cell fusion and consistently earlier observations reported that cytosolic Gal-3 is implicated as an inducer of placental cell fusion (42). Cell fusion is required for osteoclast differentiation and comprised of three steps, i.e., (i) cell–cell adhesion, (ii) cytoskeletal rearrangement, and (iii) fusion (43, 44). Previously, numbers of proteins were reported to be involved in cell fusion during osteoclast differentiation, including CD200, DC-STAMP, and E-cadherin (38, 45, 46). Adding to this list, Gal-3 was found to be located extracellularly at the cell–cell contact site where it binds with myosin-2A. Myosin-2A is a cytoskeletal protein and classified as a nonmuscle myosin, associated with cellular morphology (47). In osteoclast precursors, proteolytic inactivation of myosin-2A on the inner cell surface induced cell fusion, leading to osteoclastogenesis, indicating that myosin-2A is a suppressor of osteoclast differentiation (39). Although it is not determined how extracellular Gal-3 nullifies intracellular myosin-2A function(s), a recent study shows that extracellular Gal-3 internalizes by binding with CD44 and β1-integrin (48). Similarly, cancer-secreted Gal-3 might internalize into osteoclast cells, whereby interact with Myosin-2A. The qPCR results showed that extracellular Gal-3 affects transcriptional activities of osteoclast differentiation markers. Gal-3/myosin-2A interaction might enhance the downstream pathway of RANKL/RANK along with the fusion process. In addition, galectins generally bind to glycosylated receptors *via* conservative CRD motif. Likewise, Gal-3 interacts with integrin αM (CD11b) and integrin β2 (CD18) on the cell surface of monocytes/macrophages/osteoclast precursors (49). Thus, Gal-3–activating integrins possibly cross-talk with RANKL-mediated signaling pathways and transcription. Previously, we documented that secreted Gal-3 exerts an inhibitory effect on osteoblast differentiation through CRD-mediated Notch receptor binding (1). Taken together, cancer-secreted Gal-3 may exhibit dual properties in bone remodeling: (i) secreted Gal-3 enhances osteoclast fusion and (ii) suppresses osteoblast differentiation, leading effectively to osteolysis. Our immunohistochemistry data provide a new insight into the degradomic-peptidomic regulation in bone metastatic lesions by the profile of intact and cleaved Gal-3. Considering that Gal-3 cleavage events attenuate osteoclastogenesis, the level of Gal-3 secretion and its cleavage products could alter bone TME and may be a cause of different bone metastasis lesions in clinical observations: osteolytic (mainly breast cancer, expressing intact Gal-3), osteosclerotic (mainly prostate cancer, expressing cleaved Gal-3), and mixed lesion (50, 51). The differences of Gal-3 cleavage between breast and prostate bone metastasis may be affected by the activity of tumor-derived MMPs and/or PSA (11, 16). In addition, tissue inhibitors of metalloproteinase are expressed and α1-antichymotrypsin (ACT), a PSA inhibitor, may be generated in the host bone microenvironment (52, 53). Thus, the rate of these proteases/protease inhibitors could determine the fate of Gal-3 cleavage, ultimately creating a unique tumor-specific bone TME.

Published OnlineFirst February 2, 2016; DOI: 10.1158/0008-5472.CAN-15-1793

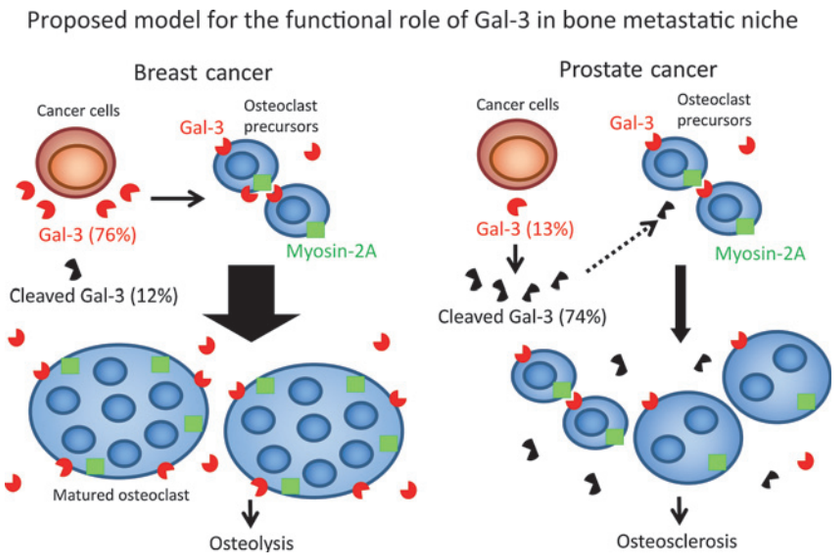

Figure 7.
A proposed model for the functional role of Gal-3 in bone metastatic niche. Left, in breast cancer bone metastasis, cancer cells secrete intact Gal-3, then Gal-3/myosin-2A interaction accelerates osteoclast cell fusion, producing mature osteoclasts and causing osteolytic bone remodeling. Right, on the other hand, in prostate cancer bone metastasis, cancer cells cleave Gal-3, which does not interact with myosin-2A, leading to attenuation of Gal-3 function on osteoclastogenesis, and consequently causes osteosclerotic bone remodeling.

Denosumab, a humanized monoclonal antibody against RANKL has been used as a first-line therapeutic drug to reduce the risk of bone destruction due to skeletal metastasis (54), but is not an ultimate treatment because the efficacy is generally limited to osteoclasts. Our data suggest a novel therapeutic modality for both bone remodeling and metastatic cancer cells. Anti-CRD antibody and/or Gal-3 antagonist reduce the bone destruction by suppressing osteoclast differentiation. In addition, Gal-3 is closely associated with cancer cell's proliferation, apoptosis, chemotherapeutic resistance, and preferable adhesion to bone marrow endothelium; therefore, Gal-3-targeting therapy may be advantageous in the quest to halt bone metastasis and progression. Meanwhile, it is important to note that prostate cancer patients do not have any antibodies that recognize the CRD (Supplementary Fig. S8), supporting a previous study in colon cancer patients (55). Therefore, therapy using anti-CRD of Gal-3 may be efficacious.

In conclusion, as depicted in Fig. 7, Gal-3 accelerates/attenuates the osteolytic vicious cycle in breast and prostate bone metastasis. The degradomic-peptidomic alteration of Gal-3, producing its cleaved form, should be considered as an integral part of bone TME. We propose a concept of "anti-osteoclast fusion" through Gal-3 targeting as therapeutic modality to promote potentially more effective bone metastasis therapy and improve patients' quality of life.

Disclosure of Potential Conflicts of Interest

No potential conflicts of interest were disclosed.

Authors' Contributions

Conception and design: K. Nakajima, T. Yanagawa, R. Mehra, A. Raz
Development of methodology: K. Nakajima, D.H. Kho, V. Hogan, R. Mehra, A. Raz
Acquisition of data (provided animals, acquired and managed patients, provided facilities, etc.): K. Nakajima, R. Ali-Fehmi
Analysis and interpretation of data (e.g., statistical analysis, biostatistics, computational analysis): K. Nakajima, D.H. Kho, W. Chen
Writing, review, and/or revision of the manuscript: K. Nakajima, D.H. Kho, T. Yanagawa, Y. Harazono, V. Hogan, R. Mehra
Administrative, technical, or material support (i.e., reporting or organizing data, constructing databases): K. Nakajima, V. Hogan, A. Raz
Study supervision: D.H. Kho, T. Yanagawa, A. Raz

Acknowledgments

The authors thank Zhi Mei (Wayne State University, Department of Chemistry, Electron Microscopy Core) for scanning electron microscopic analysis and Linda Mayernik (Wayne State University, School of Medicine, Microscopy Imaging & Cytometry Resources Core) and Paul Stemmer (Wayne State University, Proteomics Core) for mass spectrometric analyses.

Grant Support

This work was supported by NIH/NCI R37CA46120 (A. Raz), NIH Center Grant P30 ES06639 (G. Bepler), and NIH Shared Instrumentation Grant S10 OD 010700 (P. Stemmer).

The costs of publication of this article were defrayed in part by the payment of page charges. This article must therefore be hereby marked *advertisement* in accordance with 18 U.S.C. Section 1734 solely to indicate this fact.

Received July 2, 2015; revised December 22, 2015; accepted December 28, 2015; published OnlineFirst February 2, 2016.

References

1. Nakajima K, Kho DH, Yanagawa T, Harazono Y, Gao X, Hogan V, et al. Galectin-3 inhibits osteoblast differentiation through notch signaling. Neoplasia 2014;16:939–49.
2. Suva LJ, Washam C, Nicholas RW, Griffin RJ. Bone metastasis: mechanisms and therapeutic opportunities. Nat Rev Endocrinol 2011;7:208–18.
3. Manabe J, Kawaguchi N, Matsumoto S, Tanizawa T. Surgical treatment of bone metastasis: indications and outcomes. Int J Clin Oncol 2005;10:103–11.
4. Coleman R, Body JJ, Aapro M, Hadji P, Herrstedt JGroup. EGW. Bone health in cancer patients: ESMO Clinical Practice Guidelines. Ann Oncol 2014;25:124–37.
5. Liu FT, Rabinovich GA. Galectins as modulators of tumour progression. Nat Rev Cancer 2005;5:29–41.
6. Lehr JE, Pienta KJ. Preferential adhesion of prostate cancer cells to a human bone marrow endothelial cell line. J Natl Cancer Inst 1998;90:118–23.

7. Glinskii OV, Sud S, Mossine VV, Mawhinney TP, Anthony DC, Glinsky GV, et al. Inhibition of prostate cancer bone metastasis by synthetic TF antigen mimic/galectin-3 inhibitor lactulose-L-leucine. Neoplasia 2012;14:65–73.
8. Balan V, Wang Y, Nangia-Makker P, Kho DH, Bajaj M, Smith D, et al. Galectin-3: a possible complementary marker to the PSA blood test. Oncotarget 2013;4:542–9.
9. Iurisci I, Tinari N, Natoli C, Angelucci D, Cianchetti E, Iacobelli S. Concentrations of galectin-3 in the sera of normal controls and cancer patients. Clin Cancer Res 2000;6:1389–93.
10. Nangia-Makker P, Balan V, Raz A. Regulation of tumor progression by extracellular galectin-3. Cancer Microenviron 2008;1:43–51.
11. Nangia-Makker P, Raz T, Tait L, Hogan V, Fridman R, Raz A. Galectin-3 cleavage: a novel surrogate marker for matrix metalloproteinase activity in growing breast cancers. Cancer Res 2007;67:11760–8.
12. Nangia-Makker P, Wang Y, Raz T, Tait L, Balan V, Hogan V, et al. Cleavage of galectin-3 by matrix metalloproteases induces angiogenesis in breast cancer. Int J Cancer 2010;127:2530–41.
13. Balan V, Nangia-Makker P, Kho DH, Wang Y, Raz A. Tyrosine-phosphorylated galectin-3 protein is resistant to prostate-specific antigen (PSA) cleavage. J Biol Chem 2012;287:5192–8.
14. Shen Y, Liu T, Tolić N, Petritis BO, Zhao R, Moore RJ, et al. Strategy for degradomic-peptidomic analysis of human blood plasma. J Proteome Res 2010;9:2339–46.
15. López-Otín C, Overall CM. Protease degradomics: a new challenge for proteomics. Nat Rev Mol Cell Biol 2002;3:509–19.
16. Wang Y, Nangia-Makker P, Tait L, Balan V, Hogan V, Pienta KJ, et al. Regulation of prostate cancer progression by galectin-3. Am J Pathol 2009;174:1515–23.
17. Sturge J, Caley MP, Waxman J. Bone metastasis in prostate cancer: emerging therapeutic strategies. Nat Rev Clin Oncol 2011;8:357–68.
18. Onishi T, Hayashi N, Theriault RL, Hortobagyi GN, Ueno NT. Future directions of bone-targeted therapy for metastatic breast cancer. Nat Rev Clin Oncol 2010;7:641–51.
19. Smith MR, Saad F, Coleman R, Shore N, Fizazi K, Tombal B, et al. Denosumab and bone-metastasis-free survival in men with castration-resistant prostate cancer: results of a phase 3, randomised, placebo-controlled trial. Lancet 2012;379:39–46.
20. Edwards JR, Mundy GR. Advances in osteoclast biology: old findings and new insights from mouse models. Nat Rev Rheumatol 2011;7:235–43.
21. Boyle WJ, Simonet WS, Lacey DL. Osteoclast differentiation and activation. Nature 2003;423:337–42.
22. Niida S, Amizuka N, Hara F, Ozawa H, Kodama H. Expression of Mac-2 antigen in the preosteoclast and osteoclast identified in the op/op mouse injected with macrophage colony-stimulating factor. J Bone Miner Res 1994;9:873–81.
23. Seetharaman J, Kanigsberg A, Slaaby R, Leffler H, Barondes SH, Rini JM. X-ray crystal structure of the human galectin-3 carbohydrate recognition domain at 2.1-A resolution. J Biol Chem 1998;273:13047–52.
24. Mehra R, Kumar-Sinha C, Shankar S, Lonigro RJ, Jing X, Philips NE, et al. Characterization of bone metastases from rapid autopsies of prostate cancer patients. Clin Cancer Res 2011;17:3924–32.
25. Benjamini Y, Yekutieli D. The control of the false discovery rate in multiple testing under dependency. Ann Statist 2001;29:1165–88.
26. Kanda Y. Investigation of the freely-available easy-to-use software "EZR" (Easy R) for medical statistics. Bone Marrow Transplant 2013;48:452–8.
27. Kim Y, Nizami S, Goto H, Lee FY. Modern interpretation of giant cell tumor of bone: predominantly osteoclastogenic stromal tumor. Clin Orthop Surg 2012;4:107–16.
28. Li YJ, Kukita A, Teramachi J, Nagata K, Wu Z, Akamine A, et al. A possible suppressive role of galectin-3 in upregulated osteoclastogenesis accompanying adjuvant-induced arthritis in rats. Lab Invest 2009;89:26–37.
29. US National Library of Medicine. ClinicalTrials.gov [online], https://clinicaltrials.gov/ct2/show/NCT01681823 (2013), cited on March, 2015.
30. US National Library of Medicine. ClinicalTrials.gov [online], https://clinicaltrials.gov/ct2/show/NCT00514696 (2007), cited on March, 2015.
31. Nishida T, Emura K, Kubota S, Lyons KM, Takigawa M. CCN family 2/connective tissue growth factor (CCN2/CTGF) promotes osteoclastogenesis via induction of and interaction with dendritic cell-specific transmembrane protein (DC-STAMP). J Bone Miner Res 2011;26:351–63.
32. Maruyama K, Uematsu S, Kondo T, Takeuchi O, Martino MM, Kawasaki T, et al. Strawberry notch homologue 2 regulates osteoclast fusion by enhancing the expression of DC-STAMP. J Exp Med 2013;210:1947–60.
33. Grigoriadis AE, Wang ZQ, Cecchini MG, Hofstetter W, Felix R, Fleisch HA, et al. c-Fos: a key regulator of osteoclast-macrophage lineage determination and bone remodeling. Science 1994;266:443–8.
34. Takayanagi H. Induction and activation of the transcription factor NFATc1 (NFAT2) integrate RANKL signaling for terminal differentiation of osteoclasts. Dev Cell 2002;3:889–901.
35. Matsumoto M. Essential role of p38 mitogen-activated protein kinase in cathepsin K gene expression during osteoclastogenesis through association of NFATc1 and PU.1. J Biol Chem 2004;279:45969–79.
36. Minkin C. Bone acid phosphatase: tartrate-resistant acid phosphatase as a marker of osteoclast function. Calcif Tissue Int 1982;34:285–90.
37. Saftig P, Hunziker E, Wehmeyer O, Jones S, Boyde A, Rommerskirch W, et al. Impaired osteoclastic bone resorption leads to osteopetrosis in cathepsin-K-deficient mice. Proc Natl Acad Sci U S A 1998;95:13453–8.
38. Kukita T, Wada N, Kukita A, Kakimoto T, Sandra F, Toh K, et al. RANKL-induced DC-STAMP is essential for osteoclastogenesis. J Exp Med 2004;200:941–6.
39. McMichael BK, Wysolmerski RB, Lee BS. Regulated proteolysis of nonmuscle myosin IIA stimulates osteoclast fusion. J Biol Chem 2009;284:12266–75.
40. Kong YY, Feige U, Sarosi I, Bolon B, Tafuri A, Morony S, et al. Activated T cells regulate bone loss and joint destruction in adjuvant arthritis through osteoprotegerin ligand. Nature 1999;402:304–9.
41. Zhang J, Dai J, Qi Y, Lin DL, Smith P, Strayhorn C, et al. Osteoprotegerin inhibits prostate cancer-induced osteoclastogenesis and prevents prostate tumor growth in the bone. J Clin Invest 2001;107:1235–44.
42. Dalton P, Christian HC, Redman CW, Sargent IL, Boyd CA. Membrane trafficking of CD98 and its ligand galectin 3 in BeWo cells–implication for placental cell fusion. FEBS J 2007;274:2715–27.
43. Helming L, Gordon S. Molecular mediators of macrophage fusion. Trends Cell Biol 2009;19:514–22.
44. Aguilar PS, Baylies MK, Fleissner A, Helming L, Inoue N, Podbilewicz B, et al. Genetic basis of cell-cell fusion mechanisms. Trends Genet 2013;29:427–37.
45. Cui W, Cuartas E, Ke J, Zhang Q, Einarsson HB, Sedgwick JD, et al. CD200 and its receptor, CD200R, modulate bone mass via the differentiation of osteoclasts. Proc Natl Acad Sci U S A 2007;104:14436–41.
46. Mbalaviele G, Chen H, Boyce BF, Mundy GR, Yoneda T. The role of cadherin in the generation of multinucleated osteoclasts from mononuclear precursors in murine marrow. J Clin Invest 1995;95:2757–65.
47. Vicente-Manzanares M, Ma X, Adelstein RS, Horwitz AR. Non-muscle myosin II takes centre stage in cell adhesion and migration. Nat Rev Mol Cell Biol 2009;10:778–90.
48. Lakshminarayan R, Wunder C, Becken U, Howes MT, Benzing C, Arumugam S, et al. Galectin-3 drives glycosphingolipid-dependent biogenesis of clathrin-independent carriers. Nat Cell Biol 2014;16:595–606.
49. Dong S, Hughes RC. Macrophage surface glycoproteins binding to galectin-3 (Mac-2-antigen). Glycoconj J 1997;14:267–74.
50. Roudier MP, Morrissey C, True LD, Higano CS, Vessella RL, Ott SM. Histopathological assessment of prostate cancer bone osteoblastic metastases. J Urol 2008;180:1154–60.
51. Hamaoka T, Madewell JE, Podoloff DA, Hortobagyi GN, Ueno NT. Bone imaging in metastatic breast cancer. J Clin Oncol 2004;22:2942–53.
52. Kim GE, Lee JS, Choi YD, Lee KH, Lee JH, Nam JH, et al. Expression of matrix metalloproteinases and their inhibitors in different immunohistochemical-based molecular subtypes of breast cancer. BMC Cancer 2014;14:959.
53. Kikuchi E, Nakashima J, Ishibashi M, Ohigashi T, Oya M, Nakagawa K, et al. Usefulness of alpha1-antichymotrypsin-PSA complex for predicting bone metastases of prostate cancer. Urology 2007;68:371–5.
54. Brown JE, Coleman RE. Denosumab in patients with cancer-a surgical strike against the osteoclast. Nat Rev Clin Oncol 2012;9:110–8.
55. Mathews KP, Konstantinov KN, Kuwabara I, Hill PN, Hsu DK, Zuraw BL, et al. Evidence for IgG autoantibodies to galectin-3, a beta-galactoside-binding lectin (Mac-2, epsilon binding protein, or carbohydrate binding protein 35) in human serum. J Clin Immunol 1995;15:329–37.

Published OnlineFirst February 2, 2016; DOI: 10.1158/0008-5472.CAN-15-1793

Cancer Research
The Journal of Cancer Research (1916–1930) | The American Journal of Cancer (1931–1940)

AACR American Association for Cancer Research

Galectin-3 Cleavage Alters Bone Remodeling: Different Outcomes in Breast and Prostate Cancer Skeletal Metastasis

Kosei Nakajima, Dhong Hyo Kho, Takashi Yanagawa, et al.

Cancer Res 2016;76:1391-1402. Published OnlineFirst February 2, 2016.